

Kinetics of Photoelectrochemical Oxidation of Methanol on Hematite Photoanodes

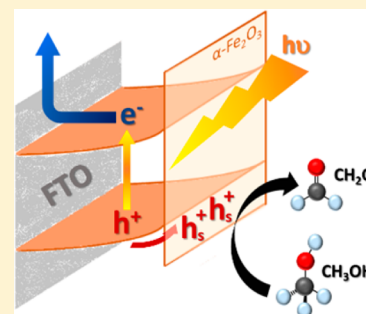
Camilo A. Mesa,[†] Andreas Kafizas,[†] Laia Francàs,[†] Stephanie R. Pendlebury,[†] Ernest Pastor,^{†,§} Yimeng Ma,[†] Florian Le Formal,^{†,‡} Matthew T. Mayer,[‡] Michael Grätzel,[‡] and James R. Durrant^{*,†}

[†]Department of Chemistry, Imperial College London, South Kensington Campus, London SW7 2 AZ, United Kingdom

[‡]Institut des Sciences et Ingénierie Chimiques, Ecole Polytechnique Fédérale de Lausanne, Station 6, CH-1015 Lausanne, Switzerland

Supporting Information

ABSTRACT: The kinetics of photoelectrochemical (PEC) oxidation of methanol, as a model organic substrate, on α -Fe₂O₃ photoanodes are studied using photoinduced absorption spectroscopy and transient photocurrent measurements. Methanol is oxidized on α -Fe₂O₃ to formaldehyde with near unity Faradaic efficiency. A rate law analysis under quasi-steady-state conditions of PEC methanol oxidation indicates that rate of reaction is second order in the density of surface holes on hematite and independent of the applied potential. Analogous data on anatase TiO₂ photoanodes indicate similar second-order kinetics for methanol oxidation with a second-order rate constant 2 orders of magnitude higher than that on α -Fe₂O₃. Kinetic isotope effect studies determine that the rate constant for methanol oxidation on α -Fe₂O₃ is retarded ~20-fold by H/D substitution. Employing these data, we propose a mechanism for methanol oxidation under 1 sun irradiation on these metal oxide surfaces and discuss the implications for the efficient PEC methanol oxidation to formaldehyde and concomitant hydrogen evolution.



INTRODUCTION

Electrochemical and photoelectrochemical (PEC) processes are widely used to drive organic oxidation reactions, with applications including molecular syntheses, photocatalytic pollutant destruction, and photoelectrochemical hydrogen generation (i.e., water splitting). For example, in PEC hydrogen generation, organic substrate oxidation can replace water oxidation as a source of electrons for proton reduction. In such systems, oxidation of sacrificial organic molecules has been shown to increase hydrogen generation yields, avoiding the kinetic limitations of water oxidation.^{1,2} Additionally, selective PEC oxidation of industrial byproducts can be used to synthesize higher value-added products. Different cases include the selective oxidation of glycerol to produce dihydroxyacetone,³ the synthesis of hydrogen and aldehydes or ketones from biomass,⁴ and epoxides from alkenes.⁵ For example, Yao and co-workers⁶ have recently reported a highly selective oxidation of various benzyl alcohols on H-titanate nanotubes. However, using photogenerated charge carriers to drive these processes can be challenging in terms of production yields and selectivity, often with only limited understanding of reaction mechanisms.⁷

In the particular case of PEC hydrogen evolution, organic substrates such as methanol or ethanol have been used to scavenge holes in metal oxide photoanodes such as TiO₂^{8,9} and α -Fe₂O₃.¹⁰ (Photo)electrochemical oxidation of methanol to formaldehyde has been reported, although with only a low Faradaic efficiency,^{11,12} with commercial formaldehyde synthesis from methanol primarily being achieved at high temperatures on iron molybdate catalysts.¹³ However, very little consideration has been given to the key kinetic and

thermodynamic parameters controlling the rate-limiting step (RLS) of PEC oxidation of methanol and their implications in the system efficiency, such as rate and yield of reaction.

This paper focuses on methanol oxidation, as a model oxidation reaction, on a widely studied photoanode material, α -Fe₂O₃, and a comparison of the kinetics of this reaction on an alternative photoanode material, TiO₂. The use of hole scavengers such as methanol has been shown to be an effective strategy to reduce electron/hole recombination losses in such metal oxides, as an alternative to the application of anodic potentials.^{10,14} Methanol oxidation studies on semiconductors such ZnO and TiO₂ have indicated a methanol adsorption process followed by the formation of a CH₃O• radical and its subsequent oxidation with a valence band hole. Other studies have provided evidence for a photocurrent doubling mechanism where methanol scavenging results in the formation of two long-lived conduction band electrons per scavenged hole. However, kinetic and mechanistic studies under operating conditions have received relatively little attention to date and are the subject of this paper.

In this study, we employ a rate law analysis to determine the key factors involved in the RLS of the methanol oxidation reaction (MOR). Such factors include different surfaces (metal oxides), the density of surface holes, and the kinetic isotope effect of deuterium (CD₃OD). The approach, following that recently employed by Le Formal et al. for water oxidation,¹⁵ employs photoinduced absorption (PIA) spectroscopy to

Received: May 19, 2017

Published: July 22, 2017

determine the density of surface holes and correlates this density with transient photocurrent (TPC) measurements under quasi-steady-state conditions of PEC methanol oxidation using long (5 s) pulsed irradiation. We provide evidence, from rate law analyses, that the kinetics of the oxidation of methanol on α -Fe₂O₃ and TiO₂ are independent of the band bending at the semiconductor–liquid junction but are instead sensitive to the choice of semiconductor and to the density of surface holes. The results presented herein allow us to propose a kinetic model and a plausible mechanism for the MOR on α -Fe₂O₃ that serves as a model for this oxidation reaction on such metal oxide photoanodes.

EXPERIMENTAL SECTION

Preparation of the Semiconductor Films. Silicon-doped α -Fe₂O₃ photoanodes were prepared by atmospheric pressure chemical vapor deposition (APCVD), by a procedure detailed elsewhere.¹⁶ These nanostructured 400 nm thick α -Fe₂O₃ films show a dendritic structure with a feature size of 5–10 nm at the surface and roughness factor of 21.

Mesoporous TiO₂ photoanodes were grown from a colloidal anatase paste, according to the method developed by Xiao-e et al.¹⁷ Mesoporous films were produced on FTO glass by doctor-blading the anatase using a k-bar followed by heat treatment at 450 °C in air for 30 min. These films were approximately 1 μ m thick with crystallites of anatase \sim 40 nm wide and roughness factor of 120.¹⁴

Photoelectrochemical Setup. A three-electrode cell was used for photoelectrochemical, photoinduced absorption spectroscopy, and transient photocurrent measurements. The electrolyte solution contained typically 0.1 M NaOH and 4% (for TiO₂) and 95% (for α -Fe₂O₃) volume methanol in deionized water. For the kinetic isotope effect (KIE) study, the electrolyte solution contained 95% CD₃OD in 0.1 M NaOD in D₂O. No concentrations higher than 98% methanol were tested due to insolubility of NaOH in such high methanol concentrations at room temperature. A Pt mesh was used as the counter electrode and a silver/silver chloride (Ag/AgCl) saturated with KCl ($E^\circ = +0.197$ V vs NHE) as the reference electrode. All potentials are reported against this Ag/AgCl electrode as the conversion of the potentials from Ag/AgCl to the reversible hydrogen electrode in highly concentrated organic aqueous solutions might not be accurate.

Linear sweep voltammograms were measured in the dark and under electrode–electrolyte (EE; front side) illumination conditions with a photon flux equivalent to approximately 100 mW·cm⁻² (1 sun) provided by two 365 nm light-emitting diodes (LEDs) (LZ1-10U600, LedEngin Inc.). The scan speed was 20 mV·s⁻¹, and the light was chopped at a frequency of 0.4 Hz.

Optoelectronic Setup. Photoinduced absorption spectroscopy allows long-lived photogenerated species to be monitored under pseudo-steady-state conditions. The PIA signal is proportional to the density of holes accumulated at the surface. Simultaneously, the transient photocurrent signal is measured in the PEC cell, by converting the potential difference between the photoanode and the counter electrode (as measured across a 98.7 Ohm resistor) into current using Ohm's law. Therefore, the TPC signal provides information on the extraction of electrons through the external circuit. The PIA and TPC signals were measured simultaneously for a 10 s period, with a 5 s on/5 s off 365 nm LED pulse. The PIA signal was measured by registering the change in the optical density (absorption) of the hematite after excitation by the UV light. The light intensity of the LEDs was varied between 0.5 and 70 mW·cm⁻² by applying a fixed current (from 0.05 to 0.70 A). This is equivalent to a photon flux of 0.06–2.7 and 0.55–5.4 suns for hematite and anatase, respectively, as calculated by Ma et al.,¹⁸ by integrating the solar power flux from the lowest limit of the measured solar spectrum to the typical absorption edge of hematite (600 nm) and anatase (380 nm). Detailed information about the PIAS and TPC measurement systems can be found in Le Formal et al.¹⁵

Formaldehyde Quantification. Formaldehyde, as methanol oxidation product, was quantified by spectrophotometric measurements. A violet color is developed by reaction between formaldehyde and 4-amino-3-hydrazino-5-mercapto-1,2,4-triazole, 4-amino-5-hydrazino-1,2,4-triazole-3-thiol (Purpald) \geq 99%, Sigma-Aldrich. A calibration curve was prepared from a concentration of 0 to 5 ppm of formaldehyde, ACS reagent, 37% W, Sigma-Aldrich, following a method developed by Jacobsen et al.¹⁹ The quantification was carried out in a PerkinElmer Lambda 25 spectrophotometer, measuring at 549 nm. The method is sensitive also to acetaldehyde, propionaldehyde, butyraldehyde, and benzaldehyde at different wavelengths; however, the only aldehyde expected from the oxidation of methanol is formaldehyde.

RESULTS

Figure 1A shows a typical current/potential (J – V) response of a nanostructured Si-doped hematite (APCVD α -Fe₂O₃) in 0.1

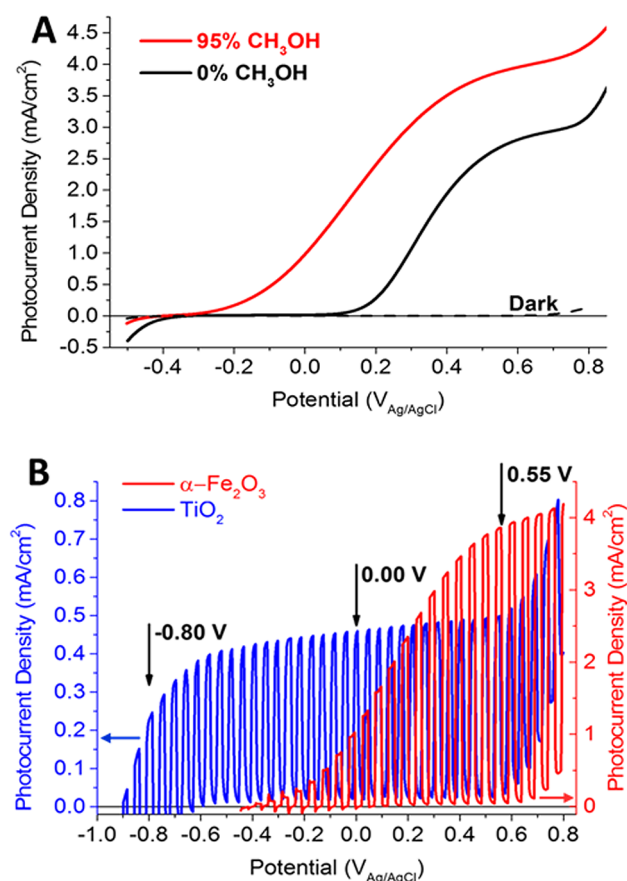


Figure 1. Current/potential response of the measured photoanodes under simulated 1 sun illumination. (a) α -Fe₂O₃ under dark (black dashed line) and front illumination conditions (electrode/electrolyte), measured in 0.1 M NaOH aqueous solution (black) and 0.1 M NaOH in 95% methanol (red) and (b) α -Fe₂O₃ (red) and anatase TiO₂ (blue) photoanodes measured in 0.1 M NaOH in 95% methanol under chopped illumination.

M NaOH and in 95% methanol in 0.1 M NaOH (see Supporting Information (SI), Figure S1, for the photocurrent response on both α -Fe₂O₃ and TiO₂ photoanodes, as a function of methanol concentration). Under simulated 1 sun illumination conditions, the photocurrent onset for the 95% methanol electrolyte, assigned below to the methanol oxidation reaction, requires approximately 270 mV less oxidative potential than that for water oxidation, consistent with previous studies.^{10,11,20}

Additionally, the oxidation of methanol produces $3.9 \text{ mA}\cdot\text{cm}^{-2}$ photocurrent at strong anodic potential ($0.55 \text{ V}_{\text{Ag}/\text{AgCl}}$) compared to $2.6 \text{ mA}\cdot\text{cm}^{-2}$ obtained from water oxidation at the same applied potential. Both the shift in the onset potential and enhancement in the plateau photocurrent are likely due to the more facile oxidation of methanol.¹⁰

Figure 1B presents comparative J - V curves under chopped illumination for the oxidation of methanol on nanocrystalline α - Fe_2O_3 versus that on mesoporous anatase TiO_2 . At high applied potentials, methanol oxidation on hematite produces an order of magnitude more photocurrent than on anatase, most likely due to better light absorption by hematite relative to titania (band gaps of 2.1 and 3.1 eV, respectively). On the other hand, titania shows a photocurrent onset approximately 500 mV cathodic of that for hematite, in accordance with their difference in the valence band edge (2.6 and 2.1 V_{NHE} at pH 14, respectively).^{21,22}

The product of methanol oxidation on hematite was determined by spectrophotometric titration. Formaldehyde was formed with a 96% Faradaic efficiency, as shown in Figure 2 (see Figures S2 and S3 for further details on the bulk

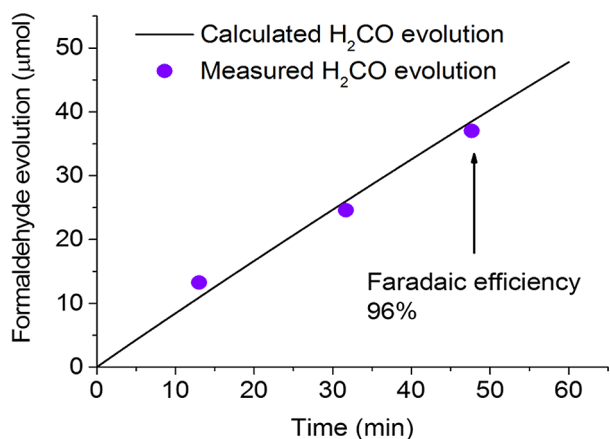
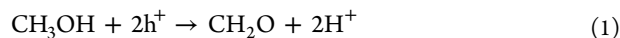


Figure 2. Formaldehyde evolution calculated from the bulk electrolysis (black line) and quantified from the calibration curve (violet circles) with a Faradaic efficiency of unity.

electrolysis and the calibration curve). This high Faradaic efficiency indicates that formaldehyde is not further oxidized to formic acid or carbon dioxide under these experimental conditions. A general equation corresponding to the oxidation can be written as follows:



where h^+ represents a surface hole on the photoanode. The strikingly high Faradaic efficiency of this reaction on hematite compared to that of an electrochemical route on Pt (81%)²³ and a photochemical process on TiO_2 , in methanol concentrations under 1% (30%),¹¹ makes this an appealing route for PEC formaldehyde synthesis.

In order to analyze the kinetics of methanol oxidation on our hematite and titania photoanodes, PIA spectroscopy and TPC measurements were conducted employing variable intensities for a duration of 5 s at 365 nm, as detailed in the Experimental Section. In these studies, the PIA signal is employed to monitor the absorbance and therefore the density of long-lived photogenerated holes, while the photocurrent density monitors the net flux of holes transferred to the electrolyte in quasi-

steady-state conditions (i.e., the rate of methanol oxidation). This approach follows that previously reported by Le Formal et al., where we have demonstrated that this PIA approach allows us specifically to probe the accumulation of long-lived holes within the depletion region at the photoanode surface and therefore assay the surface density of holes driving surface electrochemistry.¹⁵ For the PIA data, probe wavelengths of 650 and 500 nm were employed for hematite and titania photoanodes, respectively, corresponding to their valence band hole photoinduced absorption maxima.^{9,15}

Figure 3 shows the PIA (Figure 3A) and TPC (Figure 3B) responses for the oxidation of 95% methanol in 0.1 M NaOH

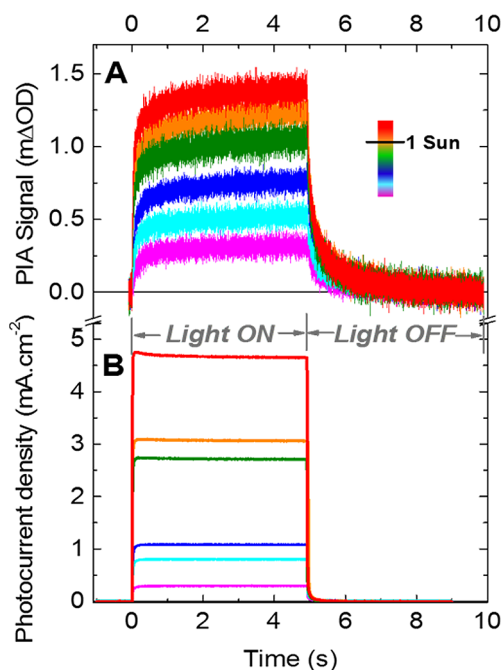


Figure 3. Oxidation of 95% methanol in 0.1 M aqueous NaOH on hematite during 5 s on/5 s off pulsed 365 nm illumination conditions at $0.55 \text{ V}_{\text{Ag}/\text{AgCl}}$. (a) Photoinduced absorption of excited species (h^+) probed at 650 nm and (b) transient photocurrent measured simultaneously.

on α - Fe_2O_3 with the photoanode held at $0.55 \text{ V}_{\text{Ag}/\text{AgCl}}$. This strongly anodic applied potential minimizes recombination in the photoanode.^{24,25} The PIA signal measured at 650 nm presented in Figure 3A shows a characteristic slow rise and plateau when the LED light is turned on and a decay when the LED light is turned off. The rise and plateau are assigned to the accumulation and reaching of a steady-state hole flux. The decay, when the light is turned off, is assigned to the dissipative reaction of long-lived hematite surface holes. These PIA rise and fall kinetics are faster than those we have reported previously for water oxidation in the absence of methanol,¹⁵ consistent with the expected faster kinetics of methanol oxidation. The steady state is reached when the flux of holes toward the surface is the same as the rate of their reaction with methanol. The photocurrent signal presented in Figure 3B exhibits faster rises and decays but similar steady-state behavior compared to the PIA signal, with the faster kinetics being assigned to fast electron extraction from the hematite film. The TPC signal drops rapidly to zero with no cathodic current spikes when the light is switched off, confirming the absence of any significant back electron/hole (or “surface”) recombination

under these strongly anodic conditions, in agreement with previous studies.^{15,24–26}

Further data analogous to those shown in Figure 3 were collected at 0.00 V_{Ag/AgCl} (see Supporting Information Figure S4A,B). Under these modest potential conditions, the attenuated space charge layer width results in less band bending (as the space charge layer is smaller than the particle size in these APCVD α -Fe₂O₃ films).²⁷ As expected, due to the resulting more severe recombination losses, higher light intensities were required to generate PIA and photocurrent signals comparable to those obtained at 0.55 V_{Ag/AgCl}. Confirming this, Figure S5 shows that at low applied potentials, back electron/hole recombination is not completely turned off and accelerates the decay kinetics of the holes accumulated at the surface of the photoanode. Furthermore, an analogous study was conducted using TiO₂ as the photoanode in 4% methanol in 0.1 M NaOH electrolyte (see Supporting Information Figure S6A,B). A lower methanol concentration was used as the photocurrent increases following methanol addition saturating at this concentration of 4% (see Figure S1). This enabled us also to monitor the titania surface hole accumulation under conditions of quasi-steady-state methanol oxidation. Before undertaking a quantitative comparison of these data, we first present the kinetic model used for their analysis.

Based on Le Formal et al.,¹⁵ we turn now to a simple kinetic model for the PEC oxidation of methanol on the photoanodes studied herein. The model is considered under steady-state conditions when the change in surface hole density, dp_s , with the time, dt , is zero (see eq 2), and the flux of photogenerated holes to the surface, $J_{\text{holes}}^{\text{sur}}$, is equivalent to the photocurrent, J_V (see eq 3).

$$\frac{dp_s}{dt} = 0 = J_{\text{holes}}^{\text{sur}} - k_{\text{MeOH}}^{\text{obs}} p_s^\alpha \quad (2)$$

$$\log(J_V) = \alpha \cdot \log(p_s) + \log(k_{\text{MeOH}}^{\text{obs}}) \quad (3)$$

where $k_{\text{MeOH}}^{\text{obs}}$ is the observed rate constant for methanol oxidation and α is the order of the methanol oxidation reaction with respect to the density of surface accumulated holes, p_s . As such, a plot of $\log(J_V)$ versus $\log(p_s)$ will have a gradient equivalent to the reaction order α . J_V can be determined from the current densities (e.g., Figure 3B) measured at 5 s after light on (i.e., quasi-steady-state conditions). The surface density of holes, p_s , can be determined at the same time from the PIA (e.g., Figure 3A) using the Beer–Lambert law from measured hole extinction coefficients at the probe wavelengths used (640 M⁻¹ cm⁻¹ for α -Fe₂O₃¹⁵ and 2000 M⁻¹ cm⁻¹ for TiO₂²⁸).

Figure 4 shows plots of the photocurrent density, J_V , as a function of the surface hole density, p_s , for the oxidation of methanol on TiO₂ and α -Fe₂O₃, employing the PIA and TPC data shown in Figure 3 and Figures S4 and S6. The data are plotted in units of nm⁻², correcting for surface roughness of the two electrodes. For all data sets, the gradients of $\log(J_V)$ versus $\log(p_s)$ are ~ 2 (within the range 1.88 to 2.13; see Figure 4), indicating that in all cases the oxidation of methanol is second order with respect to surface-accumulated holes. This second-order behavior is further supported by an initial rates law analysis (see Figure S7) of the PIA decay kinetics for methanol oxidation on hematite at 0.55 V_{Ag/AgCl}. From eq 3, we obtain second-order rate constants of 15 000 and 33 holes⁻¹ nm² s⁻¹ for TiO₂ and α -Fe₂O₃, respectively, independent of the applied

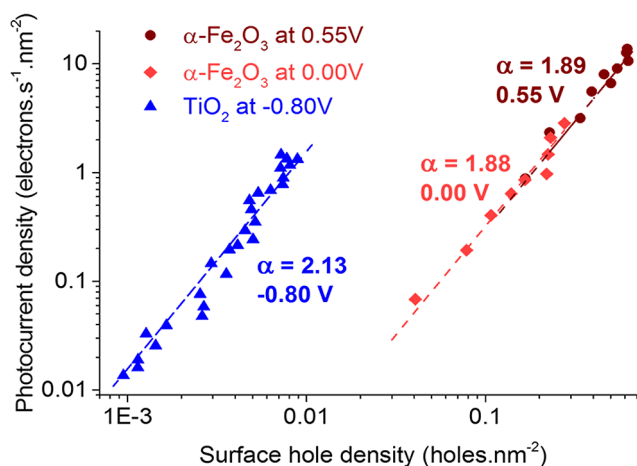


Figure 4. Rate law analysis, photocurrent density, $J_{\text{holes}}^{\text{sur}}$, and surface hole density, dp_s , of the oxidation of methanol on α -Fe₂O₃ at 0.55 V (dark red) and 0.00 V (light red) and TiO₂ (blue) at -0.80 V applied potentials.

potential. For α -Fe₂O₃ at 0.55 V_{Ag/AgCl} under conditions of approximately 1 sun irradiation (~ 4 mA cm⁻²), p_s is ~ 0.5 holes nm⁻², leading to a hole flux to the electrolyte of ~ 10 holes nm⁻² s⁻¹, corresponding to a “turnover frequency” per hole of ~ 20 s⁻¹. We further note that we obtain indistinguishable rate constants and rate laws for methanol oxidation on hematite at 0.00 and 0.55 V_{Ag/AgCl}, despite the large difference in band bending and recombination losses between these two conditions; a point we discuss in further detail below.

We undertook a kinetic isotope effect study to further analyze the kinetics and the second-order dependence of the reaction with respect to the density of accumulated holes at the surface. Therefore, we collected data analogous to that shown in Figure 3 (see Supporting Information Figure S8A,B) using deuterated 95% methanol-*d*₄ in 0.1 M NaOD in D₂O as electrolyte. Figure 5 shows the resulting rate law analysis comparing the oxidation of CH₃OH versus CD₃OD on α -Fe₂O₃. For the methanol-*d*₄ electrolyte the gradient of $\log(J_V)$ versus $\log(p_s)$ is also ~ 2 but showed a 20-fold reduction in current, compared with CH₃OH, at equivalent surface hole

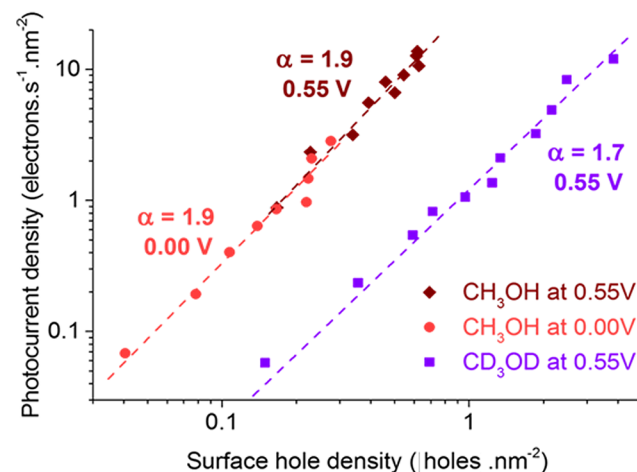


Figure 5. Kinetic isotopic effect of the oxidation of methanol on α -Fe₂O₃. Rate law analysis, photocurrent density, $J_{\text{holes}}^{\text{sur}}$, and surface hole density, dp_s , of the oxidation of CH₃OH at 0.00 V (light red) and at 0.55 V (dark red) and CD₃OD at 0.55 V (purple).

densities. The corresponding second-order rate constant for CD₃OD oxidation (1.35 holes⁻¹ nm² s⁻¹) gives a KIE of ~20, decreasing the turnover frequency per hole from ~20 to ~1 s⁻¹ under conditions of approximately 1 sun irradiation. These slower kinetics for CD₃OD oxidation indicate that the rate-limiting step of the reaction is a chemical step and involves the breaking of a C–H bond, as we discuss further below.

DISCUSSION

We have shown that, under operating photoelectrochemical oxidation conditions, methanol is fully oxidized to formaldehyde on both TiO₂ and α -Fe₂O₃ with a rate that depends on the square of the density of surface-accumulated holes, by quasi-steady-state kinetic analysis of the reaction. We note this result differs from our analysis of water oxidation on identical α -Fe₂O₃ (see Figure S9), where we observed first-order behavior with respect to p_s at low surface hole densities transitioning to third-order behavior at high hole densities.¹⁵ Moreover, the kinetics of the methanol oxidation reaction depend upon the metal oxide surface chemistry, as well as the presence of deuterium in the electrolyte, but are independent of the applied potential.

We first focus on the hematite data collected at two different applied potentials. It is striking that our plots of J_V versus p_s collected at 0.00 and 0.55 V_{Ag/AgCl} overlay each other, showing the same reaction order and rate constant with respect to surface hole density. These reaction conditions are very different, with severe surface electron/hole recombination losses at 0.00 V_{Ag/AgCl}²⁴ but no surface recombination at 0.55 V_{Ag/AgCl}. Although water oxidation does not occur at 0.00 V_{Ag/AgCl}, it is possible that it becomes competitive with methanol oxidation at high applied potentials; however, this is ruled out by Supporting Information Figure S9. The agreement between 0.00 and 0.55 V_{Ag/AgCl} data confirms the validity of our experimental protocol and that our analysis does indeed address the kinetics of methanol oxidation at the semiconductor/electrolyte interface. We observe that at equivalent surface hole densities, the kinetics of methanol oxidation are independent of applied potential, clearly demonstrating that the kinetics of the reaction are not determined by the electrode Fermi level or band bending. Rather this observation indicates that these kinetics are simply determined by the density of holes accumulated at the electrode surface, with an energy determined by the valence band edge. This situation is consistent with the semiconducting nature of hematite and contrasts the behavior of metal electrodes, where changing the applied potential changes the free energy driving the reaction.^{21,29}

Turning now to the comparison of titania and hematite shown in Figure 4, it is apparent that titania shows methanol oxidation kinetics ~500-fold faster than that of hematite, despite the lower “photocurrent-saturating” methanol concentration (4% in titania compared to 95% in hematite, as shown in Figure S1). This difference in the concentration of methanol needed to reach the maximum photocurrent densities has been suggested to depend on a competitive mechanism of adsorption between water and methanol on anatase,³⁰ compared to hematite where a strong chemisorption of methanol (as methoxide) has been reported.³⁰ This difference in concentration dependence may also be related to the lower Faradaic efficiencies reported for methanol oxidation on TiO₂ (e.g., 30% reported by Wahl et al.¹¹ for the oxidation of 0.4% methanol in 0.1 M NaOH). Despite these differences, it is striking that

methanol oxidation on titania also exhibits second-order behavior as a function of surface hole density, suggesting some similarity in the reaction mechanism. A full analysis of methanol oxidation on titania and its dependence on, for example, methanol concentration is beyond the scope of this study. Nevertheless, it is clear that methanol oxidation on titania is at least 2 orders of magnitude faster than that on hematite. These faster kinetics can be most obviously assigned to the deeper valence band edge of TiO₂ relative to α -Fe₂O₃ (2.6 and 2.1 V_{NHE} at pH 14, respectively),^{21,22} providing a larger energy offset to drive the methanol oxidation reaction, although we note that differences in methanol surface adsorption may also be important.

A two-step methanol oxidation mechanism on oxide surfaces has been proposed previously in the context of observations of photocurrent doubling for similar systems.^{31,32} This pathway of reaction begins with the adsorption of a molecule of methanol on the metal center, releasing a proton. Subsequently, a surface hole is transferred to the adsorbed methoxide, forming a methoxy radical, which then undergoes a second oxidation step by injection of an electron into the conduction band of the photoanode, producing formaldehyde.^{11,23,31} This photocurrent doubling mechanism (where one photon generates two conduction band electrons) has been observed previously under low light intensity conditions on TiO₂ and ZnO.^{11,32,33} However, we note that Schoenmakers et al.³³ have reported a reduction in the quantum efficiency of methanol oxidation on ZnO from 2 to 1 when increasing the light intensity from ~0.005 to 5 suns. The results we report here provide an explanation for Schoenmakers et al.’s observation and indicate that under ~1 sun irradiation conditions, where there is significant hole accumulation at the oxide surface, both steps of methanol oxidation are driven by photogenerated valence band holes. These results in the observed second-order dependence on surface hole density and no significant current doubling effect are in agreement with previous reports operating at ~1 sun conditions.^{12,34}

We finally focus on the KIE shown in Figure 5. The aforementioned methanol adsorption on the photoanode surface leads to the loss of the H atom from the O–H bond. Therefore, our observation of a KIE of ~20 is most obviously assigned to a C–H bond breaking in the rate-limiting step of methanol oxidation. We note that this would be an unusually high KIE value for a C–H bond breaking considering only the stretching mode of this bond (KIE_{Expected} ~ 7).³⁵ However, C–H bond breaking of surface-bound CH₃O• species will be associated with significant structural changes and specifically a change in the carbon hybridization from sp³ to sp². This rehybridization can be expected to lead to considerable differences in the zero-point energy of the transition state due to the loss of stretching as well as bending modes.^{35–37} Therefore, we conclude that the rate-limiting step in the oxidation of methanol under conditions of ~1 sun illumination and alkaline electrolyte involves the breaking of a C–H bond and an associated rehybridization of the carbon.

Based upon these data and previous literature studies,^{11,12,20,23,31–34,38} we propose a mechanism for methanol oxidation on hematite and titania photoanodes, as shown in Figure 6. We note that Grassian and co-workers³⁹ have determined the “saturating” methanol-adsorbed surface density on α -Fe₂O₃ to be ~2 × 10¹³ molecules·cm⁻², corresponding to one molecule of methanol adsorbed every 5 nm² on α -Fe₂O₃, which is comparable to our measured surface hole densities

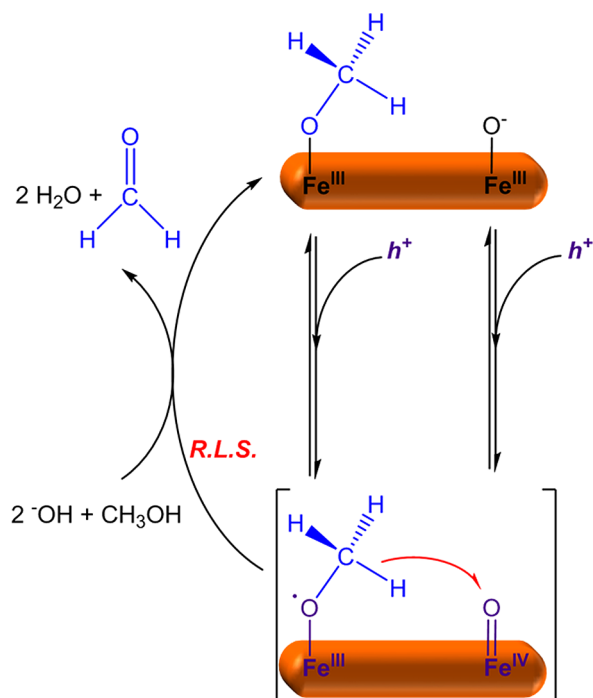


Figure 6. Plausible mechanism of methanol oxidation on $\alpha\text{-Fe}_2\text{O}_3$, where the RLS requires oxidations by two valence band holes and involves C–H bond breaking, leading to rehybridization of the carbon to produce formaldehyde with a Faradaic efficiency of unity; h^+ refers to surface valence band holes (Fe(IV)=O species not adjacent to adsorbed methanol).

($\sim 5 \times 10^{13} \text{ h}^+ \cdot \text{cm}^{-2}$ under 1 sun irradiation). This reported methanol coverage allows us to rule out direct interactions between adsorbed methanol molecules. As such, we assign the RLS in our observed second-order methanol oxidation to be the oxidation of a surface-adsorbed methoxy radical with a hematite surface valence band hole, as illustrated in Figure 6. We note that our observation of second-order methanol oxidation indicates that the concentration of methoxy radicals scales with the surface hole density, implying that under steady-state conditions an equilibrium is formed between these species. This mechanism is also consistent with the observation of methoxy radicals during methanol oxidation on oxide surfaces that has been reported previously.^{11,23,31,38} Surface hematite holes have been assigned previously to Fe(IV)=O species;⁴⁰ methanol oxidation requires two of these species to diffuse together to form the reactive species, as indicated in Figure 6. This mechanism is in accordance with our observed second-order behavior under technologically relevant conditions reported herein of 1 sun illumination. Our observation of a similar, second-order, rate law for methanol oxidation on TiO_2 suggests that the same reaction mechanism is also likely to operate on this metal oxide, with the higher rate constant resulting from the deeper valence band in titania compared to hematite.

CONCLUSIONS

The use of organic oxidation substrates can substantially reduce the requirement of strong anodic potentials for PEC hydrogen evolution, as well as potentially enable the synthesis of useful organic compounds. As a study case, we have reported kinetic and mechanistic analyses for the selective oxidation of a model substrate, methanol to formaldehyde, on titania and hematite

photoanodes under PEC working conditions. The methanol oxidation reaction was found to be second order with respect to the density of surface holes, indicating a reaction mechanism where both steps of methanol oxidation are driven by valence band holes. The second oxidation, involving a C–H bond breaking, is the rate-limiting step. Remarkably, this oxidation is observed to proceed with near unity Faradaic efficiency, suggesting a potentially attractive route to formaldehyde synthesis from methanol. Our observation of second-order behavior also has important implications for technological applications, as it implies that the kinetics and therefore potentially the efficiency of this widely used reaction will be superlinearly dependent upon the surface density of accumulated holes, with implications for photoanode design (e.g., surface area) and optimum operational light intensities.

ASSOCIATED CONTENT

Supporting Information

The Supporting Information is available free of charge on the ACS Publications website at DOI: 10.1021/jacs.7b05184.

Current–voltage curves for different concentrations of methanol in 0.1 M NaOH on $\alpha\text{-Fe}_2\text{O}_3$ and TiO_2 ; formaldehyde quantification details; PIA and TPC signals measured at 0.00 V for hematite and -0.80 V for anatase, as well as PIA and TPC signals for the oxidation of CD_3OD on hematite at 0.55 V; effect of recombination on PIA decays, an initial rates analysis for methanol oxidation, and a comparison of rate law analysis for water and methanol oxidation (PDF)

AUTHOR INFORMATION

Corresponding Author

*j.durrant@imperial.ac.uk

ORCID

Camilo A. Mesa: 0000-0002-8450-2563

Andreas Kafizas: 0000-0002-2282-4639

Laia Francàs: 0000-0001-9171-6247

Yimeng Ma: 0000-0002-7826-5338

Michael Grätzel: 0000-0002-0068-0195

James R. Durrant: 0000-0001-8353-7345

Present Address

[§]Physical Biosciences Division, Lawrence Berkeley National Laboratory, Berkeley, California 94720, USA.

Notes

The authors declare no competing financial interest.

ACKNOWLEDGMENTS

We acknowledge Dr. Robert Godin for helpful discussions and financial support from the European Research Council (project Intersolar 291482), Swiss National Science Foundation (project 140709) and Swiss Federal Office for Energy (project PECHouse 3, contract number SI/500090-03). C.A.M. thanks COLCIENCIAS for funding; L.F. thanks the EU for a Marie Curie fellowship (658270), and E.P. thanks the EPSRC for a DTP scholarship.

REFERENCES

- (1) Kudo, A.; Miseki, Y. *Chem. Soc. Rev.* **2009**, *38*, 253.
- (2) Li, X.; Yu, J.; Low, J.; Fang, Y.; Xiao, J.; Chen, X. *J. Mater. Chem. A* **2015**, *3*, 2485.

- (3) ten Brink, G.; Arends, I. W. C. E.; Sheldon, R. A. *Science* **2000**, *287*, 1636.
- (4) Palmisano, G.; Garcia-Lopez, E.; Marci, G.; Loddo, V.; Yurdakal, S.; Augugliaro, V.; Palmisano, L. *Chem. Commun.* **2010**, *46*, 7074.
- (5) Kasap, H.; Caputo, C. A.; Martindale, B. C. M.; Godin, R.; Lau, V. W.; Lotsch, B. V.; Durrant, J. R.; Reisner, E. *J. Am. Chem. Soc.* **2016**, *138*, 9183.
- (6) Yang, J.; Shen, X.; Wei, J.; Zhang, L.; Zhao, D.; Yao, B. *Catal. Sci. Technol.* **2016**, *6*, 7604.
- (7) Ruberu, T. P. A.; Nelson, N. C.; Slowing, I. I.; Vela, J. J. *Phys. Chem. Lett.* **2012**, *3*, 2798.
- (8) Antoniadou, M.; Lianos, P. *Appl. Catal., B* **2010**, *99*, 307.
- (9) Kafizas, A.; Wang, X.; Pendlebury, S. R.; Barnes, P.; Ling, M.; Sotelo-Vazquez, C.; Quesada-Cabrera, R.; Li, C.; Parkin, I. P.; Durrant, J. R. *J. Phys. Chem. A* **2016**, *120*, 715.
- (10) Pendlebury, S. R.; Barroso, M.; Cowan, A. J.; Sivula, K.; Tang, J.; Grätzel, M.; Klug, D.; Durrant, J. R. *Chem. Commun.* **2011**, *47*, 716.
- (11) Wahl, A.; Ulmann, M.; Carroy, A.; Jermann, B.; Dolata, M.; Kedzierzawski, P.; Chatelain, C.; Monnier, A.; Augustynski, J. *J. Electroanal. Chem.* **1995**, *396*, 41.
- (12) Micka, K.; Gerischer, H. *J. Electroanal. Chem. Interfacial Electrochem.* **1972**, *38*, 397.
- (13) Soares, A. P. V.; Portela, M. F.; Kiennemann, A. *Catal. Rev.: Sci. Eng.* **2005**, *47*, 125.
- (14) Wang, X.; Kafizas, A.; Li, X.; Moniz, S. J. A.; Reardon, P. J. T.; Tang, J.; Parkin, I. P.; Durrant, J. R. *J. Phys. Chem. C* **2015**, *119*, 10439.
- (15) Le Formal, F.; Pastor, E.; Tilley, S. D.; Mesa, C. A.; Pendlebury, S. R.; Grätzel, M.; Durrant, J. R. *J. Am. Chem. Soc.* **2015**, *137*, 6629.
- (16) Kay, A.; Cesar, I.; Grätzel, M. *J. Am. Chem. Soc.* **2006**, *128*, 15714.
- (17) Xiao-e, L.; Green, A. N. M.; Haque, S. A.; Mills, A.; Durrant, J. R. *J. Photochem. Photobiol., A* **2004**, *162*, 253.
- (18) Ma, Y.; Pendlebury, S. R.; Reynal, A.; Le Formal, F.; Durrant, J. R. *Chem. Sci.* **2014**, *5*, 2964.
- (19) Jacobsen, N. W.; Dickinson, R. G. *Anal. Chem.* **1974**, *46*, 298.
- (20) Klahr, B.; Gimenez, S.; Zandi, O.; Fabregat-Santiago, F.; Hamann, T. *ACS Appl. Mater. Interfaces* **2015**, *7*, 7653.
- (21) Nozik, A. J.; Memming, R. *J. Phys. Chem.* **1996**, *100*, 13061.
- (22) Chen, S.; Wang, L.-W. *Chem. Mater.* **2012**, *24*, 3659.
- (23) Batista, E. A.; Malpass, G. R. P.; Motheo, A. J.; Iwasita, T. *J. Electroanal. Chem.* **2004**, *571*, 273.
- (24) Le Formal, F.; Pendlebury, S. R.; Cornuz, M.; Tilley, S. D.; Grätzel, M.; Durrant, J. R. *J. Am. Chem. Soc.* **2014**, *136*, 2564.
- (25) Peter, L. *J. Solid State Electrochem.* **2013**, *17*, 315.
- (26) Peter, L. M. *Chem. Rev.* **1990**, *90*, 753.
- (27) *Photoelectrochemical Hydrogen Production*; van de Krol, R., Grätzel, M., Eds.; Springer: New York, 2012.
- (28) Cowan, A. J.; Leng, W.; Barnes, P. R. F.; Klug, D. R.; Durrant, J. R. *Phys. Chem. Chem. Phys.* **2013**, *15*, 8772.
- (29) Bard, A. J.; Faulkner, L. R. *Electrochemical Methods: Fundamentals and Applications*, 2nd ed.; John Wiley & Sons, Inc.: New York, 2001.
- (30) Wang, C.-Y.; Groenzin, H.; Shultz, M. J. *J. Am. Chem. Soc.* **2005**, *127*, 9736.
- (31) Zhou, C.; Ren, Z.; Tan, S.; Ma, Z.; Mao, X.; Dai, D.; Fan, H.; Yang, X.; LaRue, J.; Cooper, R.; Wodtke, A. M.; Wang, Z.; Li, Z.; Wang, B.; Yang, J.; Hou, J. *Chem. Sci.* **2010**, *1*, 575.
- (32) Fermin, D. J.; Ponomarev, E. A.; Peter, L. M. In *Proceedings of the Symposium on Photoelectrochemistry*; Rajeshwar, K., Ed.; The Electrochemical Society: Pennington, NJ, 1997; Vol. 97.
- (33) Schoenmakers, G. H.; Vanmaekelbergh, D.; Kelly, J. J. *J. Chem. Soc., Faraday Trans.* **1997**, *93*, 1127.
- (34) Nomikos, G. N.; Panagiotopoulou, P.; Kondarides, D. I.; Verykios, X. E. *Appl. Catal., B* **2014**, *146*, 249.
- (35) Anslyn, E. V.; Dougherty, D. A. *Modern Physical Organic Chemistry*; University Science Books: Sausalito, CA, 2006.
- (36) Stewart, R.; Van der Linden, R. *Tetrahedron Lett.* **1960**, *1*, 28.
- (37) Westheimer, F. H. *Chem. Rev.* **1961**, *61* (3), 265.
- (38) Shen, M.; Henderson, M. A. *J. Phys. Chem. Lett.* **2011**, *2*, 2707.
- (39) Carlos-Cuellar, S.; Li, P.; Christensen, A. P.; Krueger, B. J.; Burrichter, C.; Grassian, V. H. *J. Phys. Chem. A* **2003**, *107*, 4250.
- (40) Zandi, O.; Hamann, T. W. *Nat. Chem.* **2016**, *8*, 778.